Materials Letters 136 (2014) 345–348

Contents lists available at ScienceDirect

Materials Letters

journal homepage: www.elsevier.com/locate/matlet

High barium content lead and alkaline-free glasses

Maviael J. Da Silva [a], José S. Moya [b,*], Carlos Pecharromán [b], Jesús Sanz [b], Sonia Mello-Castanho [a]

[a] IPEN/Universidade de Sao Paulo, Sao Paulo, Brazil
[b] ICMM-CSIC, Madrid, Spain

ARTICLE INFO

Article history:
Received 13 February 2014
Accepted 16 August 2014
Available online 26 August 2014

Keywords:
Refraction index
Ba-Glasses
Lead-Free glasses

ABSTRACT

Four glass compositions of the system BaO-Al_2O_3-SiO_2 with high content of BaO > 50% mol and with B_2O_3 addition (3–10 wt%) were melted at 1400 °C. The effect of alkaline earth BaO oxide on the glass phase separation and on refraction index n is investigated. IR and MAS-NMR spectroscopy are used for structural characterization. Finally stable alkaline free glasses with a content of BaO ranging from 47.4 Mol.% to 54.5 Mol.% and with a $n = 1.62 \pm 0.01$ at 468.1 nm have been obtained.

Recently, the need and opportunities for new glasses in different emerging technologies such as solid-state lighting, i.e., higher-refractive-index substrates or light-extraction coatings, photovoltaic, energy-efficient windows and batteries have been reported [1,18,19]. In this context, free-alkaline glasses with a high content of BaO can find important technological added value applications.

Batch compositions with high content of BaO ($\geq$70 wt%) presents the phenomena of immiscibility and phase separation and consequently are very difficult to be fabricated and the availability of reliable phase-diagram information is necessary [2,3]. Although lead glasses display many technological advantages, lead is a toxic metal with a wide range of biological effects [4]. The main purpose of the present work is to obtain and characterize stable, high homogeneity, transparent, colorless and eco-friendly glasses, lead and alkaline-free, with high Ba^{2+} content $\geq$ 47 Mol.%, displaying high refractive index ($n \geq 1.6$) in the system RO-Al_2O_3-SiO-B_2O_3(R=Ba).

Four glass compositions labeled B47, B49, B52, and B54 were selected taking into account the BaO-SiO_2-Al_2O_3 equilibrium diagram [16,17] as well as the compatibility triangle (BS-B2S-BAS2) [3]. In selected compositions, the amount of BaO (R^{2+} glass modifier) ranges from (47–55) Mol.%, Al_2O_3 (3–6) Mol.%, and SiO_2 (30–36) Mol.%. Boron oxide was added (4.8 to 15.6 Mol.%) in order to decrease the melting point of the selected batch compositions (Table 1).

Raw materials in adequate proportion for 40 g batch were mixed and melted in a platinum crucible at 1400 °C for 2 h in a vertical furnace then quenched in a pre-heated metallic mold. Subsequently, glasses were annealed at 50 °C below their glass transition temperature (Tg). The density, ρ, of the investigated glass samples was measured at room temperature by the Archimedes method.

The powdered glass samples (20–40 μm) were characterized by X-ray diffractometry (XRD). All the compositions showed X-ray peak-free patterns (not show). The refractive index was obtained by spectral ellipsometry using an ellipsometer SOPRA GES-5E, with a micro-spot facility, equipped with an Xe lamp covering the spectral range from 190 nm to 2000 nm at an incidence angle of 65°. The samples size after cutting and polishing was about $(10 \times 10 \times 10)$ mm^3.

For the determination of the glass structure a FT-IR Bruker IFS-66V was used. The samples were grinded to powder to mix with KBr and then pressed at 500 MPa to obtain a pellet. The spectral range covered was from 250 cm^{-1} to 4000 cm^{-1}. High-resolution MAS-NMR experiments were performed at room temperature in a Bruker Avance 400 spectrometer operating at 79.48 MHz (^{29}Si signal), 104.26 MHz (^{27}Al), and 128.38 MHz (^{11}B). ^{29}Si (I=1/2), ^{27}Al (I=5/2) and ^{11}B (I=3/2) MAS-NMR spectra were recorded after $\pi/2$ pulse irradiation (5, 2, and 3.5 μs, respectively). Glass powders were packed into zirconia rotors. The spin rate was 10 kHz. The number of scan was 800 for silicon, 400 for aluminum and 200 for Boron. Time intervals between successive accumulations were chosen as 10.5 and 5 s. The ^{29}Si, ^{27}Al, and ^{11}B chemical shifts were measured using tetramethylsilane (TMS) and $AlCl_3$ and H_3BO_3 solutions as external references. The experimental errors were $\pm$0.5 ppm for the three NMR signals.

Differential Scanning Calorimetry (DSC) of glass samples was carried out in air at 10 °C min^{-1}. The softening temperature (Tg) and the thermal expansion coefficient (α) of the bulk glasses and final glass–ceramics were measured in air with a Netzsch

* Corresponding author.
E-mail address: jsmoya@icmm.csic.es (J.S. Moya).

http://dx.doi.org/10.1016/j.matlet.2014.08.094
0167-577X/

dilatometer at 10 °C min^{-1}, with cylindrical samples of length ~15 mm and diameter 5 mm.

The DSC curves for all the glassy samples reveal that glass transition and crystallization temperatures increase with Al_2O_3 content, acting as glass former, hence increasing Tg (onset of glass transition) and Tp (first crystallization peak). In the present glasses, the amount of modifier is high owing to the existence of a large number of non-bridging oxygen ions; in this case, Al^{3+} cations can attain a coordination number of 6, and so non-bridging oxygen converts into bridging oxygen with the addition of Al_2O_3 by replacing B_2O_3. Therefore, the conversion of non-bridging oxygen to bridging oxygen leads to increase in Tg and Tp of these glasses [2,14]. The significant difference between Tp and Tg (227 °C) defined in terms of resistance to crystallization of the glass during heating, displayed by the sample labeled B52, means the large ability of the glass to flow [2,5]. The thermal properties, Tg, Tp and TECs values of all glasses are presented in Table 1.

The FT-IR absorbance spectra of the investigated glasses are shown in Fig. 1a. Four main broad absorbance bands in the region of 300 to 1500 cm^{-1} can be detected in all spectra. The lack of any sharp feature is an indicative of the degree of amorphization of the silicate network due to the generalized distribution of Qn units [5–7]. The spectral modes of these samples can be tentatively assigned as follows: while the high frequency band could be assigned to Boron vibrations, the three remaining low frequency maximum can be found in most of the silica-based glasses, and more specifically in those with Celsian composition [10] suggesting that the structure of both glasses must be similar. In the particular case of the highest frequency band, it should be noted that it presents some structure (two definite maxima at 1425 and 1395 cm^{-1}) in the B54 sample. These peaks are absent in the B52 sample, while in two Barium poorer glasses, a shoulder was detected around 1260 cm^{-1}. The most intense IR band covers a broad spectral range from 1200 to 800 cm^{-1}. This mode is customary assigned to the stretching vibrations of Si-O-Si linkages. In this respect, it is noticeable the fact that for the lower Barium content samples (B47 and B49) this band is asymmetric, which could suggest the presence of distorted SiO_4 tetrahedral. Finally, the lower frequency band, located from 600 to 300 cm^{-1}, corresponds to bending vibrations of Si-O-Si.

In the highest Barium content sample, the phase segregation is produced where the Boron-rich component will be the crystalline

Table 1
Glass compositions (% Molar); bulk density, ρ; Glass (Tg) and exothermic peak (Tp) temperatures; Thermal Expansion Coefficient (TEC); refractive index at 486.1 nm and Abbe number.

Sample ID	Composition (Mol.%) (R=Ba)	Density (gcm^{-3})	TG (°C)	Tp (°C)	TEC (10-6 °C-1)	n (468.1 nm)	νd
B54	54.5 RO-3.3 Al2O3-35.7 SiO2-6.5 B2O3	3.8	641	866	9.7	1.59	229
B52	52.3 RO-4.9 Al2O3-38.0 SiO2-4.8 B2O3	3.8	661	887	10.5	1.62	94
B49	49.2 RO-4.8 Al2O3-31.8 SiO2-14.1 B2O3	3.4	644	787	9.6	1.62	78
B47	47.4 RO-6.4 Al2O3-30.7 SiO2-15.6 B2O3	3.3	624	781	8.8	1.62	53

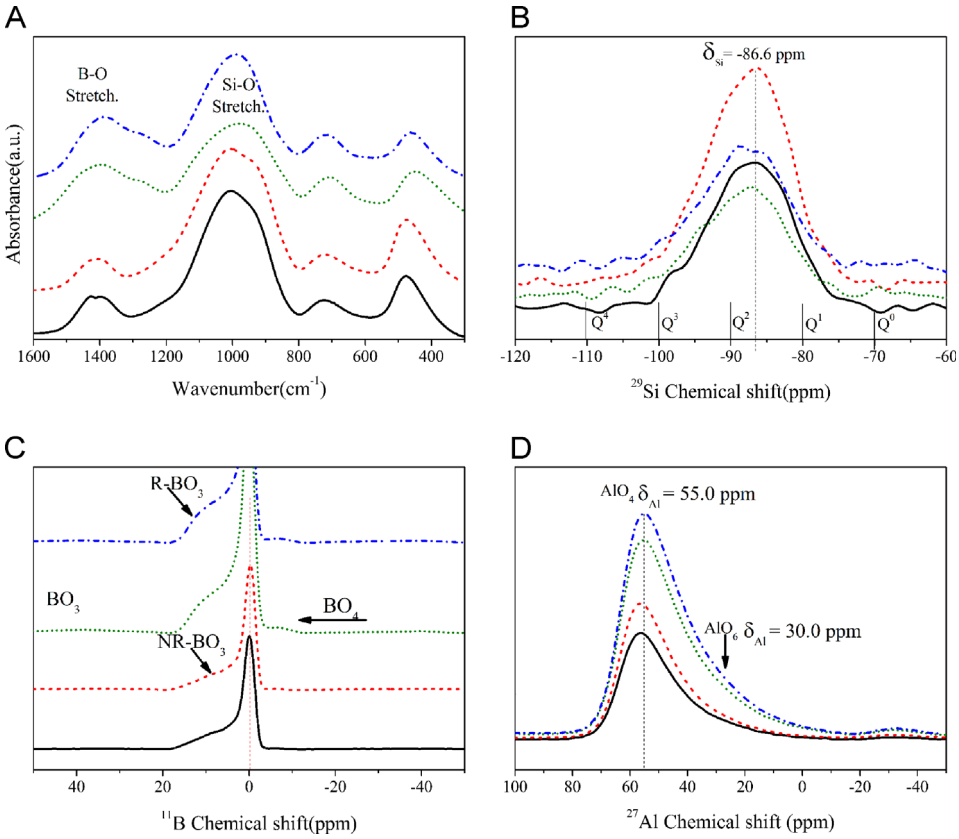

Fig. 1. Structural spectroscopic spectra (IR and NMR) of the considered glasses. For all the four graphics the black continuous line corresponds to B54 sample, the red dashed to B52, the green dotted to B49 and the blue dashed-dotted to the B47 sample. Subplot (a) stands for IR absorption spectra; (b) for 29Si NMR; (c) for ^{11}B NMR; and (d) for ^{27}Al NMR spectra.

phase. The IR modes of this phase will correspond to the definite modes detected around 1400 cm^{-1}. As far as the Barium content is reduced, Boron oxide and silica polyhedral start to coordinate forming O-B-O-Si-O covalent structures (which present a vibration band around 1265 cm^{-1}), stabilizing the glass. The ^{29}Si MAS-NMR spectra of the as-prepared parent glasses (B47 to B54) are shown in Fig. 1b. In all compositions, the main component of spectra display chemical shift values centered about −86.6 ppm, indicating that tetrahedral Q^1 (dimers) and Q^2 (short chains) units dominate in the glass network [5,8–10]. One Ba^{2+} neutralizes two NBO oxygen (Non Bridging Oxygen), suggesting that the alkaline earth oxides provide a stronger network linkage than alkaline cation on glassy networks [11–14]. When the glass compositions are modified by addition of alkaline earth oxides (Fig. 1d), trigonal BO_3 is converted to tetrahedral BO_4 reaching a maximum at ≈54.5 Mol.% BaO (B54). Above this composition, the BO_3 units are re-converted into BO_4 [12].

Reversal trend occurs in the variation of density, Tg, TEC, and refractive index. This effect is the so-called boron anomaly. The tetrahedral BO_4 is not associated with NBO and the connectivity of tetrahedra gives rise to open structures for ≥52.3 Mol.% BaO compositions. Conversely, for compositions ≤52.3 Mol.% BaO, BO_4 units break and BO_3 units are formed; as a consequence there is a network disrupt and consequently a better occupied volume. This new structural environment increases the trend to change TEC, Tg, and refractive index [21,22].

The obtained ^{27}Al MAS-NMR spectra of parent glasses (Fig. 1c) present two main peaks: (i) a resonance centered at 55.0 ppm, which is characteristic of AlO_4 tetrahedral units in Celsian ($BaAl_2Si_2O_8$), and (ii) another small one at 32.0 (AlO_5) associated with pentahedral aluminum. From peak intensities, AlO_4 units seem to be favored in prepared glasses.

From NMR results, we have deduced that aluminum and Boron atoms have mainly adopted the fourfold coordination. The structure of these high Ba content glasses is not far from that proposed by Djordjevic et al. [10] for barium aluminosilicate glasses with celsian stoichiometry, where double tetrahedral layers (SiO_4-BO_4-AlO_4) were reported [11].

The optical properties at the UV–vis range of obtained glasses were measured by spectroscopic ellipsometry. This technique is only valid for single phase samples [9,15]. It should be noted that heterogeneities, such as secondary phase or precipitates (with a particle size comparable to the incident wavelength) depolarize the reflected light and, consequently, the quality of the measurements becomes unacceptable. In this sense, in Fig. 2A–D, the optical micrographs of the polished surfaces of the four studied glass compositions appear. In Fig. 2A and B, corresponding to the highest BaO content samples, heterogeneities are clearly visible associated to phase separation processes, while in samples with the BaO content below 50 Mol.%, the surface appears to be homogeneous (Fig. 2C and D).

In the case of a relative amount of heterogeneities, such as secondary phase or precipitates appear in the samples, the light scattering phenomena depolarize the reflected light and consequently, the quality of measurements becomes unacceptable. In this regard, the quality of the data measured by this technique has been employed in this work as an indication of the phase segregation. In Fig. 2E both experimental (n exp) and fitted (n calc) refractive indices are plotted versus wavelength for all studied glasses.

For sake of comparison, we have used the three-oscillator Sellmeier equation [13] described as:

$$n^2-1=\frac{A_1\lambda^2}{\lambda^2-B_1}+\frac{A_2\lambda^2}{\lambda^2-B_2}+\frac{A_3\lambda^2}{\lambda^2-B_3} \quad (1)$$

Eq. (1) incorporates two UV–vis oscillators and one IR oscillator to take into account the resonant mode that appears in the near-IR range. However, on the herewith considered samples, we found that just a single term was enough to obtain satisfactory fittings. We included both fittings as numerical values of refractive index at selected wavelengths (Table 2). The obtained refractive index of these glasses is quite high, $n=1.62$, so that, in addition with its easy polishing, it makes this material a good candidate to be used to fabricate optical glasses [5,9,14,20]. However, not all the fittings have attained a similar quality. While the samples with lower Barium content present a very good fit (B47and B49), when the Barium content approaches to the solubility limit, the optical quality of the samples deteriorates (Fig. 2), and the goodness of

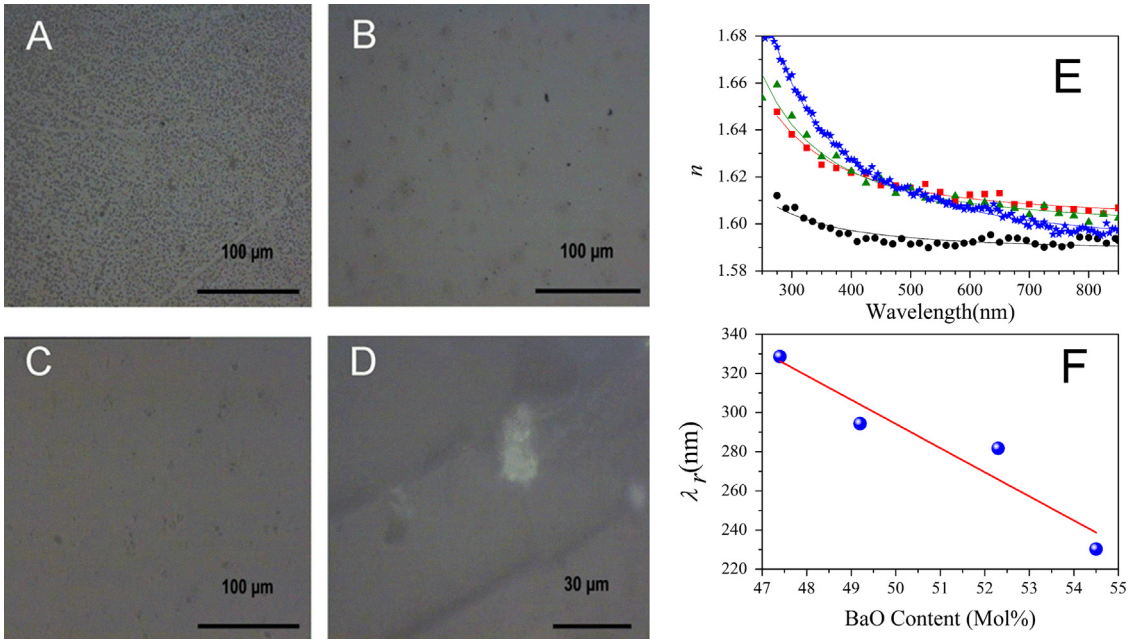

Fig. 2. Optical microscopy micrographs of the glass samples and refractive index measurements: (A) B54 optical micrograph showing phase separation with droplets. The same for (B) B52 sample; (C) B49 sample; (D) B47 sample; (E) refractive index dispersion determined by spectroscopic ellipsometry and their fittings using a Sellmeier relationship corresponding to B54 (●), B52 (■), B49(▲) and B47 (★) samples; (F) UV wavelength resonance vs. Barium content for all glass samples.

Table 2
Sellmeier coefficients, A, B, and the optical parameter (λ_r): wavelength resonance.

Glass ID	A1	B1	A2	B2	A3	B3	λ_r Resonance Wavelength (nm)
B54	1.110	6.18E-02	0.414	3.2E-4	0.971	103.6	230
B52	1.187	8.26E-02	0.380	6.78E-2	1.086	103.6	282
B49	1.184	8.66E-02	0.371	8.66E-2	1.025	103.6	294
B47	1.168	1.08E-01	0.360	1.08E-1	1.086	103.6	329

fitting considerably drops, as a consequence of secondary phase inclusions and bubbles.

Moreover, another remarkable property of these glasses is its low dispersion. In the present case, the more relevant term is the one associated to the band-gap absorption located in the near UV. The wavelength resonance can be estimated to be the square root of the B term in the Sellmeier equation (considering just a single oscillator). In Fig. 2F, the UV wavelengths resonance versus the Barium content is depicted.

According to this plot, the relationship between both magnitudes is linear. In this sense, as low the UV spectral range is, the lower the dispersion will be. Therefore, the Ba role in the optical properties is double: (i) it increases the refractive index, due to its large electron density, and (ii) it enlarges the transparency window and simultaneously reduces the dispersion in the optical spectral region.

From a technical point of view, dispersion is described by the Abbe number ($\nu_d=(n_d\text{-}1)/(n_F\text{-}n_C)$). In Table 1, we have included the obtained values of ν_d for the four Ba glasses. Generally speaking, all the samples presented considerable large values of the Abbe numbers which in addition to their high refractive index allow to classify then as Crown glasses [22] ($n_d > 1.60$, $\nu_d > 50$). In fact, by composition, the studied samples would correspond to the SK or SSK glass types (dense and extra dense barium crown) but in the present case they display larger values of the Abbe parameter. It may be due to the presence of alumina in the atomic network which allows a homogeneous packing, in a similar way as the crystalline hexacelsian [10].

In summary, it has been proven that it is possible to fabricate alkaline-free glasses with high refraction index (≥ 1.6) from batch compositions following a narrow range of stoichiometry: (47 to 55 Mol.%) BaO; (3–6 Mol.%) Al_2O_3; (30–38 Mol.%) SiO_2 and (4.8–16 Mol.%) B_2O_3, through a reasonably low melting temperature of 1400 °C. These lead-free glasses have been fabricated at workable melting temperature, using low cost raw materials. Because of this the obtained glasses can be considered promising materials for optical systems and very competitive versus the ones with similar optical properties based on expensive rare-earth raw materials.

Acknowledgments

This work has been supported by the Brazilian CNPq (237958/2012-0), Spanish MINECO (MAT2010-19837-06 and MAT2011-29174-C02-01) and CSIC, Spain (201360E012).

References

[1] Pantano CG, Jain H, Bange K. Am Ceram Soc Bull 2013;92(8):30–3.
[2] Navarro JMF. El. Vidrio, CSIC, Madrid, 2003.
[3] Semler CE, Foster WR. J Am Ceram Soc 1970;53(11):595–8.
[4] ATSDR. Draft toxicological profile for lead. Atlanta, GA, Agency for Toxic Substances and Disease Registry, (⟨http://www.atsdr.cdc.gov/toxprofiles/tp13⟩; 2005 [accessed 02 09 13].
[5] Samuneva B. J Non-Cryst Solids 1991;129:54–63.
[6] Doweidar H. J Non-Cryst Solids 2000;277:98–105.
[7] Higby PL, Aggarwal ID. J Non-Cryst Solids 1993;163:303–8.
[8] Habs D, Gunther MM, Jentschel M, Urban W. Phys Rev Lett 2012;108:1–4.
[9] Masai H, Ueno T, Takahashi Y, Fujiwara T. Opt Mater 2011;33:1980–3.
[10] Djordjevic J, Dondur V, Dimitrijevic R, Kremenovic. Phys Chem 2001;3:1560–5.
[11] Sutrisno A, Lu C, Lipson RH, Huang Y. J Phys Chem 2009:21196–201.
[12] Stebbins JF, Zhao P, Kroeker S. Solid State Nucl Mag 2000;16(1–2):9–19.
[13] Sellmeier W. Annalen der Physik 1871:7–9.
[14] Stepanov L. Rev Adv Mater Sci 2011;27:115–45.
[15] Fasasi AY, Maaza M, Rohwer EG, Knoessen D, Leitch A, Buttner U. Thin Solid Films 2008;516:6226–32.
[16] Doweidar H. J Non-Cryst Solids 1998;240:55–65.
[17] Doweidar H. J Non-Cryst Solids 2011;357:1665–70.
[18] Petit L, Carlie N, Chen H, Gaylord S, Massera J, Boudebs G, et al. J Solid State Chem 2009;182:2756–61.
[19] Buchner S, Pereira MB, Balzaretti NM. Opt Mater 2012;34:826–31.
[20] Abdel-baki M, Wahab FA, El-Diasty F. Chem Phys 2006;96:201–10.
[21] Zhong J, Xiang W, Chen Z, Zhao H, Liang X. Mater Sci Eng B 2013;178:998–1003.
[22] Marvin J Weber. Handbook of optical materials. (Chapter 2). Boca Ratón: CRC PRESS; 2002.